



Fabrication, characterization, dielectric properties, thermal stability, flame retardancy and transport behavior of chlorinated nitrile rubber/hydroxyapatite nanocomposites

A. Nihmath¹ · M. T. Ramesan¹

Received: 9 May 2020 / Revised: 2 July 2020 / Accepted: 6 November 2020 /
Published online: 16 November 2020
© Springer-Verlag GmbH Germany, part of Springer Nature 2020

Abstract

This work focused on the preparation of chlorinated nitrile rubber (Cl-NBR)/hydroxyapatite (HA) nanocomposites by an open two-roll mixing mill. The formation of nanocomposites was characterized by Fourier transform infrared (FTIR), X-ray diffraction (XRD), scanning electron microscopy (SEM) and thermogravimetric analysis (TGA). The dielectric properties and flame retardancy of polymer nanocomposites were analyzed with special attention to the loading of HA nanoparticles. Diffusion and permeation properties of petroleum solvents through the prepared Cl-NBR/HA composites were also investigated in detail as a function of filler content, different temperatures and nature of solvent. The incorporation of HA in Cl-NBR has been endorsed by FTIR analysis. The XRD showed the crystalline peaks of HA in the polymer chain. SEM images revealed that the nanoparticles were uniformly distributed in the polymer network with spherically shaped particles. TGA results indicated that the thermal stability of nanocomposites was remarkably higher than the pure Cl-NBR and the thermal stability increases with the loading of nanoparticles. The dielectric study observed a decreasing dielectric constant with increasing frequency, and the maximum property was obtained for 7 phr HA filling in Cl-NBR. The flame resistance of the polymer composites was greatly enhanced by the incorporation of nanoparticles. The diffusion, sorption and permeation constants were found to decrease with increase in HA content. The solvent uptake decreases with the size of the penetrant molecules, and the mechanism of transport of Cl-NBR composite was anomalous in nature. The enthalpy and entropy changes of the nanocomposites were analyzed from the diffusion data. The composite containing 7 phr HA sample showed higher dielectric properties and better solvent resistance properties.

Keywords Chlorinated NBR · Structure · Crystallinity · Flame resistance · Thermal stability · Dielectric properties · Transport properties

✉ M. T. Ramesan
mtramesan@uoc.ac.in

Extended author information available on the last page of the article

Introduction

Over the last two decades, nanocomposites open a new perspective in the field of science to upgrade the structural and functional properties of existing polymers. The inherent high surface area of nanomaterials increases their dispersion capability in the matrix which offers ample scope for the improvement in properties as compared to conventional micro- and macrocomposites [1, 2]. Many investigations are carried out for the processing of thermoplastic elastomer-based composites with enhanced performance without recourse to expensive synthetic procedures [3, 4]. Also, earlier articles on this topic have indicated that the physical and chemical interaction of fillers with the rubber matrix, the crosslinking chemistry of rubber, nature of nanofillers are the key factors affecting the processability and performance of elastomeric nanocomposites [5, 6]. It is a great task to configure appropriate density of crosslinking networks in material because it determines the elasticity, mechanical reinforcements and solvent resistance of rubbers. It was reported that noncovalent chemical bond and supramolecular interactions such as metal ion crosslinking, electrostatic attractions seem to improve the properties of elastomer-based composite [7, 8].

Different research work was carried out on NBR-based composites using various kinds of nanofillers such as nanoclay, nanosilica, nanocalcium carbonate, carbon nanotube [9–11]. Composite of NBR with waste dispersion phases from fly ash powder was used for the production of high strength materials in polymer industry [12]. In the majority of these works the effective reinforcement is achieved by the surface modification of fillers with organo-modifiers through ion exchange reactions since the strong interparticle interaction in nanomaterials due to high surface energy and the hydrophobicity of rubber is not favorable for blending of these two phases [13]. Reported studies on matrix-modified elastomer composites are scarce. Previous studies revealed that the polarity and hydrophilicity of elastomer surface can be considerably improved by simple and inexpensive chlorination and result in a product with enhanced chemical and mechanical properties. The chloro group will increase the compatibility of filler with the matrix [14].

Higher demand for environmental protection along with new technology and business opportunities leads to a continuous increase of research on bioresorbable polymer nanocomposite [15]. It includes either a biodegradable matrix or filler. There are a lot of reports based on polymer/HA composite materials [16]. Dong et al. investigated the thermal properties and flame retardancy behavior of polycarbonate/hydroxyapatite nanocomposite [17]. Bhowmik et al. studied the load-carrying behavior of polymer and response of interfaces when the load is applied in ex situ HAP composites using MD and SMD simulations [18]. Hydroxyapatite acts as nucleating agent for crystallization of polyamide and also improved the osteogenic and morphological characteristics of polyamide composite, reported by Velazco et al. [19].

This work focused on the fabrication of Cl-NBR/HA nanocomposites by simple, inexpensive two-roll mixing techniques. The structural characterization,

morphology and thermal behavior of new Cl-NBR/HA nanocomposites were done by Fourier transform infrared spectroscopy (FTIR), X-ray diffraction (XRD), scanning electron microscopy (SEM) and thermogravimetric analysis (TGA). The electrical properties such as dielectric constant and dielectric loss tangent were also evaluated with respect to the different loading of nanoparticles. Moreover, this work demonstrates the effect of nanohydroxyapatite on the transport properties of chloro-functionalized NBR.

Experimental

Materials and methods

The nitrile rubber with 18% acrylonitrile content was purchased from Synthetics and Chemicals Ltd, UP, India. Tetrabutyl ammonium bromide (TBAB), chloroform (CHCl_3), sodium hydroxide (NaOH), dicumyl peroxide (DCP), toluene, calcium chloride (CaCl_2), ammonium hydrogen phosphate ($(\text{NH}_4)_2\text{HPO}_4$), ammonium hydroxide (NH_4OH) and isopropyl alcohol were obtained from Merck, India. For the diffusion studies, the solvents such as petrol (mol. wt. 100), kerosene (mol. wt. 170) and diesel (mol. wt. 230) were procured from Bharat Petroleum Corporation Limited, India.

Synthesis of chlorinated NBR (Cl-NBR)

Chlorinated NBR (22% chlorine) was prepared through a phase transfer catalysis method as described previously [20]. Briefly, nitrile rubber was dissolved in toluene and it was then mixed with TBAB and CHCl_3 . Aqueous NaOH solution was added drop by drop to the above reaction mixture and stirred it for 8 h. Chlorinated NBR was separated from the solution by coagulating with isopropyl alcohol and finally dried.

Preparation of hydroxyapatite (HA) nanoparticles

A simple co-precipitation technique was used for the preparation of hydroxyapatite nanoparticles [21]. Briefly, the aqueous solution of CaCl_2 and $(\text{NH}_4)_2\text{HPO}_4$ was mixed under vigorous stirring. NH_4OH was added to the reaction mixture and stirred it for 24 h. The precipitate formed was filtered and washed. Finally, the hydroxyapatite (HA) particles were sintered at 600 °C for 6 h.

Preparation of Cl-NBR/HA nanocomposites

The Cl-NBR/HA nanocomposites were prepared by a simple two-roll mill mixing technique. Cl-NBR was first masticated for 6 min, followed by the addition of different loading of nano-HA powder (0, 3, 5, 7, 10 and 15 phr). The crosslinking agent DCP (6 phr) was incorporated in accordance with the ASTM D-15-627 method with

special attention paid to maintain the uniform mixing of filler in the rubber matrix. The prepared samples were named as N0 for unfilled Cl-NBR, N3, N5, N7, N10 and N15 for Cl-NBR with 3, 5, 7, 10 and 15 phr of HA-filled rubber nanocomposites.

Characterization

Fourier transform infrared spectrophotometer (JASCO 4100 model FTIR) in the range 400–4000 cm^{-1} was used to explore the formation of Cl-NBR/HA nanocomposite. XRD patterns of HA and Cl-NBR/HA composites were recorded using a Rigaku D/MAX 2200 Model X-ray diffractometer operated 2θ range of 10–70° at a scanning speed of 1°/min. The surface morphology of Cl-NBR composites was analyzed by Hitachi SU 6600 scanning electron microscope (SEM). Thermal property analysis of Cl-NBR with different contents of HA particles were performed using a PerkinElmer Pyris 1 under the nitrogen atmosphere at a heating rate of 10 °C/min and at a flow rate of 100 mL/min from 25 to 650 °C. The dielectric properties of polymer composites were measured by a fully automatic Hewlett Packard LCR meter (HP: 4284A) at different frequencies. The diffusion and transport mechanism of Cl-NBR/HA nanocomposites was carried out by using a circular-shaped vulcanized sheet, and these samples were immersed in various solvents, like petrol, diesel and kerosene taken in the diffusion bottles. The solvents absorbed by the composites were weighed at particular time intervals and again inserted in the solvents. The weighing of the sample was continued up to equilibrium weight obtained. These studies were carried out at different temperatures, and the diffusion experiments were conducted duplicates or triplicates in most cases.

Results and discussion

FTIR Spectroscopy

The chemical structure characteristics of Cl-NBR/HA nanocomposite are identified by Fourier transform infrared (FTIR) spectroscopic measurement, and all the spectra are given in Fig. 1. The IR spectrum of Cl-NBR shows characteristic bands of nitrile group, butadiene segment and dichlorocarbene group. Chlorinated NBR shows absorption peaks at 802 cm^{-1} (assigned to C–Cl stretching vibration), 1062 cm^{-1} (corresponding to cyclopropyl ring) along with significant absorption at 2239 cm^{-1} are the characteristic–CN stretching vibration. The bands at 972 cm^{-1} and 692 cm^{-1} are the corresponding –CH stretching vibration of cis and trans counterparts of butadiene segment, respectively [20, 22]. The –OH stretching and bending vibrations of hydroxyapatite nanoparticles are present at 3482 cm^{-1} and 1683 cm^{-1} due to OH stretching and OH bending vibrations, respectively. The ν_1 , ν_2 , ν_3 and ν_4 vibration modes of phosphate group present in HA are obtained at 940, 540, 789 and 665 cm^{-1} , respectively [23]. The FTIR peaks of Cl-NBR/ HA nanocomposites are manifested by most of the peaks present in both Cl-NBR and HA nanoparticle with a slight shift in the absorption. For example, the major peak of HA at 540 cm^{-1}

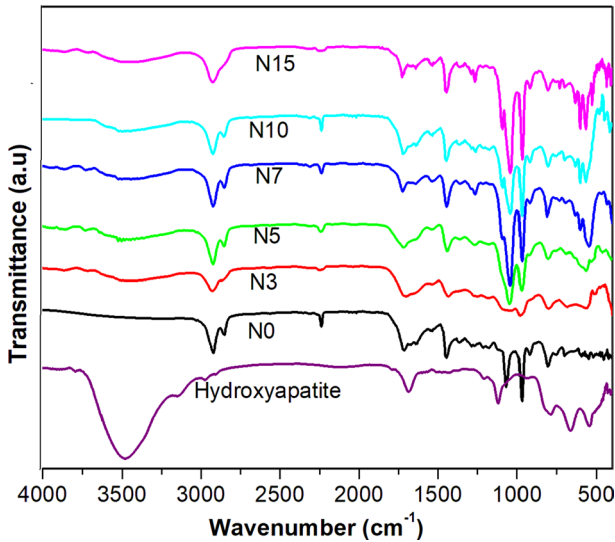


Fig. 1 FTIR spectra of CI-NBR and different contents of HA-filled CI-NBR

is found to be shifted to 567 cm^{-1} . A significant increase in intensity of 557 cm^{-1} can be observed from Fig. 1 (N5 to N15). IR absorption spectra reveal that increasing HA content induces more efficient interaction between HA and CI-NBR chains. In addition to this, the chlorinated absorption band of CI-NBR is slightly shifted from at $802\text{--}811\text{ cm}^{-1}$ by the insertion of nanoparticles in the macromolecular chain of CI-NBR. Similarly, the CN stretching of the sample also shifts from at $2239\text{--}2230\text{ cm}^{-1}$. These shifts in polar segments of rubber after the inclusion of nanoparticles clearly indicated that the polar group of nanoparticles undergo strong intermolecular interaction with the chlorinated segment of NBR.

X-ray diffraction analysis (XRD)

X-ray diffraction pattern of hydroxyapatite and CI-NBR is given in Fig. 2. The different diffraction peaks of hydroxyapatite obtained at $2\theta = 25.7^\circ, 31.6^\circ, 32.7^\circ, 34.1^\circ, 39.7^\circ, 46.6^\circ, 49.5^\circ$ and 53.09° are the diffraction of (002), (211), (300), (202), (310), (222), (213) and (321) crystal planes, respectively [21]. The XRD peak of CI-NBR shows that the 2θ value at 19.85° indicates its amorphous region, and a weak reflection at $2\theta = 40.72^\circ$ is the chlorinated segment of NBR. Figure 3 shows the XRD profile of various loading of HA-filled CI-NBR composites. The XRD pattern of CI-NBR with HA particles retained all the peaks of HA nanoparticles with the amorphous peak of CI-NBR. The intensity of the XRD peaks of HA in the polymer increases with an increase in the loading of nanoparticles and reveals that the nanoparticles are uniformly located in the macromolecular chain of the composite matrix. The ordered arrangement of nanoparticles in the polymer matrix is due to the strong intermolecular interaction between the hydroxyl group of HA with polar segments of CI-NBR. The average particle size of 5, 7, 10 and 15 phr dosage of

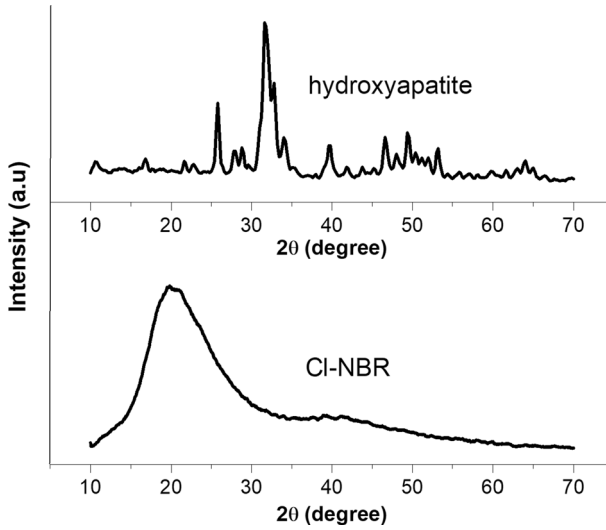


Fig. 2 XRD patterns of HA nanoparticles and CI-NBR

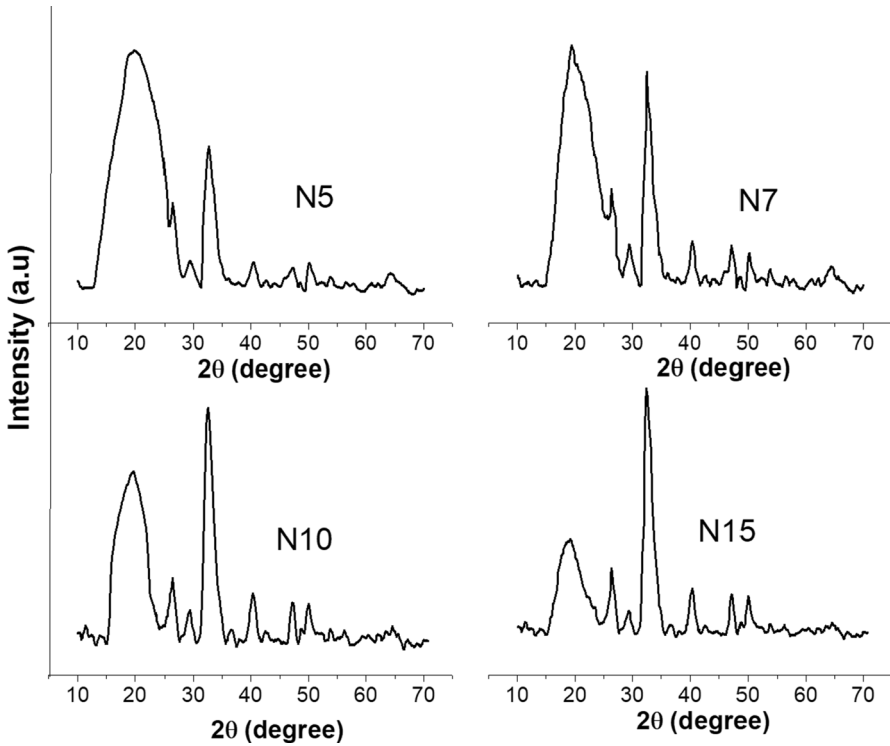


Fig. 3 XRD patterns of different contents of hydroxyapatite-filled CI-NBR

HA-filled CI-NBR rubber was estimated automatically from corresponding XRD data using Scherrer formula, $D=0.89\lambda/\beta \cos \theta$, and the average particle size is 23.62, 27.58, 27.97 and 31.89 nm, respectively. It can be seen from the figure that the amorphous peak of CI-NBR ($2\theta=19.85^\circ$) is slightly shifted to a lower diffraction angle at $2\theta=19.36^\circ$ and also the amorphous region of polymer decreases with the addition of nanoparticles. This shift in XRD peak along with the reduction in amorphous region of composite is an evidence for the formation of nanocomposite. A dilution effect is operated during the effective mixing of crystalline nanofiller with the amorphous CI-NBR which leads to the shift or reduction in amorphous region of the polymer matrix. Besides, the proportion of effective amorphous component decreases with the increase in content of HA particles during the processing of polymer composites. The percentage of crystallinity induced by the dispersion of 5, 7, 10 and 15 phr of hydroxyapatite nanoparticles in the rubber is found to be 46.53%, 56.62%, 65.58% and 77.41%, respectively.

Scanning electron microscopy (SEM)

The morphology of the fabricated composite materials was evaluated by using scanning electron microscopy. The SEM micrographs of CI-NBR and CI-NBR with different contents of HA nanoparticles are presented in Fig. 4. It is reported that [20] chlorination of matrix induces surface roughening is paralleled by a reduction in surface friction [Fig. 4 (N0)]. From the micrograph, it is visible that in the lower loaded sample [Fig. 4 (N3 and N5)], the nanoparticles are more dispersed in the jaggy matrix with few stacks of HA, while the surface morphology is changed into a uniform structure [Fig. 4 (N7)] as the loading of nanoparticles reached to 7 phr. This uniform dispersion of filler is due to the polar interaction between rubber matrix and $-\text{OH}$ group of the nanoparticles. In addition to this, the increased surface area provides more sites for interlocking of HA particles in the polymer composite. This will enhance the homogenous distribution of nanoparticles in the polar rubber. As

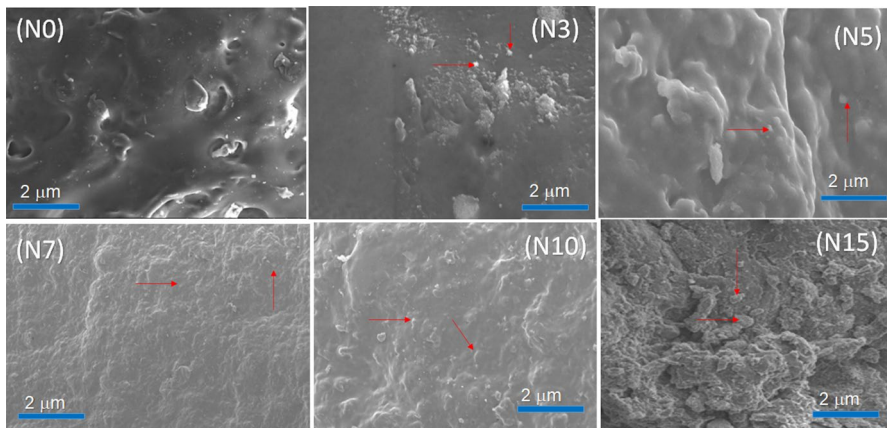


Fig. 4 SEM images various loading of HA-filled CI-NBR

the HA content increases to 10 phr in Fig. 4 (N10), the uniform dispersion of filler is slightly changed into a wavy nature with the initiation of flocculation tendency of the nanoparticles that is due to the stress developed in the composite material. A cluster-like morphology is clearly visible at higher loading (15 phr) of filler [Fig. 4 (N15)]. This behavior is attributed to the strong interparticle interaction through hydroxylated edge which will extend the interface and the increased domain size and thereby decreases the interfacial interaction between matrix and filler. These agglomerated HA heaps create an irregular structure in CI-NBR/15phr HA composite.

Thermogravimetric analysis (TGA)

In TGA, the loss in weight after decomposition due to the formation of volatile products is monitored as a function of temperature. The TGA curves of CI-NBR and CI-NBR/HA nanocomposites with different contents of HA are given in Fig. 5. All the samples show a minor and major thermal decomposition pattern. The minor decomposition of all samples is assigned to the removal of hydrogen chloride and the compounding ingredients from the polymer. The major rubber degradation is the cleavage of long-chain molecules and producing short polymer chains. It is well clear from the figure that the degradation rate of nanocomposites is very slow as compared to the degradation of neat CI-NBR and the thermal stability of the composite increases with the loading of nanoparticles. This is due to the homogeneously incorporated hydroxyapatite nanoparticles having a high aspect ratio that may hinder the thermal degradation of rubber in the earlier stages of decomposition by acting as a superior insulator. The significant weight loss delay is attributed to the intimate contact between rubber and HA through polar attraction which may slow down the volatilization as well as assist the formation of char after decomposition. The volatile products generated retard the diffusion of oxygen into the polymer matrix and

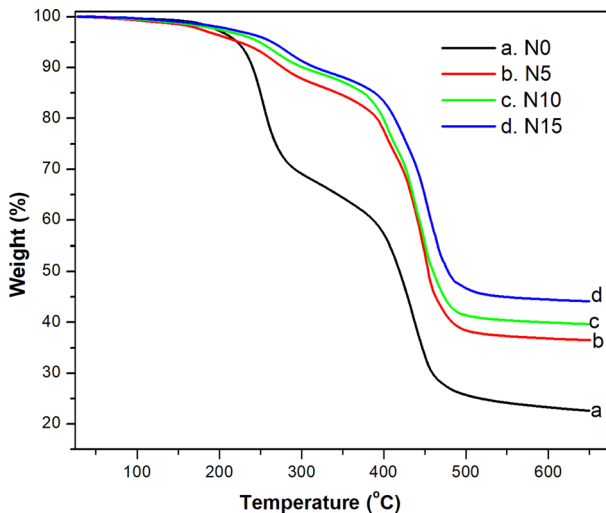


Fig. 5 TGA thermograms of CI-NBR and CI-NBR/HA nanocomposites

shift the decomposition to a higher temperature and thus increase the thermal stability of the nanocomposites [24]. At a temperature of 650 °C, the chlorinated NBR has a residue of 22.53%, whereas 5, 10 and 15 phr of HA-loaded composite, char residues are 36.59%, 40.12% and 44.78%, respectively, at the same temperature. The char residue of polymer composite is higher than the neat Cl-NBR and showed that hydroxyapatite acts as char promoter, thereby enhancing the flame retardant of the composite system.

Flame retardancy

Flame test (LOI) is widely used to evaluate the flame-retardant properties of polymer composites. The LOI values of Cl-NBR with 0, 3, 5, 7, 10 and 15 phr HA-loaded samples are 27.6, 28.4, 30, 32, 33.8 and 35, respectively. The unfilled Cl-NBR rubber showed the lowest LOI value among all composite materials. The flame resistant of the nanocomposite increased with the loading of nanoparticles. The interaction of halogenated components of NBR with hydroxyapatite nanoparticles retards the burning of the polymer. Also, during the burning of polymer, a thick char is coming out from the halogenated polymer (intumescent effect) which protects the surface of the polymer from further burning [25]. The amount of char layer is less at lower loading of nanoparticles; hence, it cannot act as an efficient barrier. On the other hand, the content of char layer formed at the polymer surface is higher at higher loading which leads to higher LOI values. Thus, it can be concluded that the HA particles can impart better flame resistance to chlorinated NBR.

Dielectric constant

Dielectric measurement detects the fluctuation of dipoles derived from atomic, electronic, interfacial and orientation polarization. Figure 6 compares the variation of relative dielectric constant (ϵ_r) with frequency for Cl-NBR and Cl-NBR/HA nanocomposites having different loading of HA at room temperature. It is obvious that at a lower-frequency region a strong dispersion of permittivity is observed, while at higher frequency ϵ_r becomes nearly constant. The sharp decrease in dielectric constant with an increase in frequency may be attributed to the electrical relaxation processes which are the result of lag in the orientation polarization [26, 27]. That is the orientation of dipoles belonging to different polar groups takes more response time to reach the equilibrium static field compared with electronic and atomic polarization. The Cl-NBR/HA nanocomposites show higher dielectric values than the neat Cl-NBR. This may be due to the presence of large number of permanent dipoles spontaneously following the direction of polarization which increases with the increase in filler content. The dielectric constant of rubber composite increases with the loading of nanoparticles up to 7 phr. The strong interaction between the polar groups of HA and the chlorinated segment of NBR reduces the cohesive force of macromolecular chains which enhances the dielectric constant [28]. This result suggests that the polymer and HA nanoparticles are compatible due to the interactions between them and the shear stresses generated during the processing of rubber

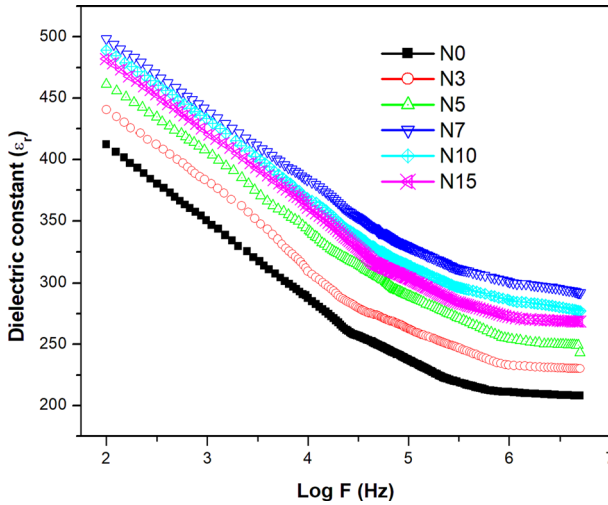


Fig. 6 Dielectric constant of CI-NBR and CI-NBR /HA nanocomposites

nanocomposite. The decrease in dielectric constant beyond 7 phr loading is due to the formation of small clusters in the nanocomposite (which is well clear from the SEM analysis) which resist the segmental mobility of the elastomeric chains [29].

Dielectric loss ($\text{Tan}\delta$)

It is generally believed that dielectric data of elastomer nanocomposite provide information on molecular relaxation of the polymer backbone. Figure 7 shows the

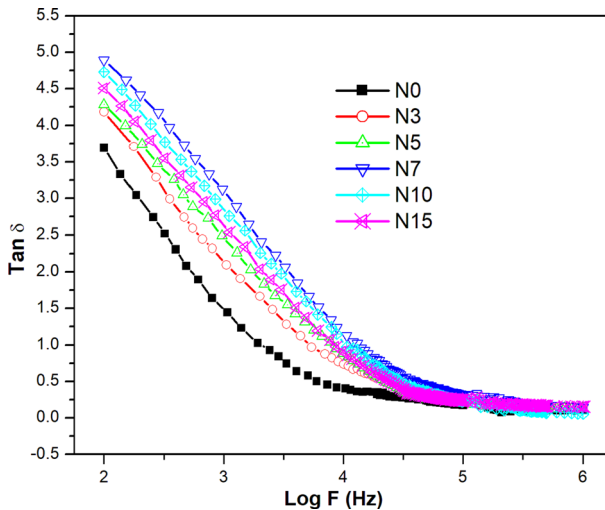


Fig. 7 Dielectric loss of CI-NBR with various contents of HA-filled CI-NBR

variation of dielectric loss with the frequency of CI-NBR and CI-NBR/HA nanocomposites having different loadings of HA at room temperature. Dielectric loss decreases rapidly with increase in frequency up to 10^5 Hz and then decreases slowly that shows low loss with further increase in frequency. Dielectric loss may occur by the localized motion of charge carriers [30, 31]. The higher dispersion of dielectric loss at lower frequency is attributed to the easy flow of charge carriers within the materials due to their low inertia and binding forces between the molecules [32]. Beyond a certain critical frequency, the exchange energy of dipoles connected with electric charge carriers in the system cannot follow the alternation of applied AC frequency. Specifically, being a function of relaxation process dielectric loss increases with an increase in filler loading due to interfacial polarization [33]. The difference in conductivity of CI-NBR and HA leads to local displacement of electrons in the direction of applied electric field which induces polarization at the anchoring region of filler and polymer matrix. The conductive network thus formed will allow easy motion of trapped charge carriers through the electrically heterogeneous system so that $\tan \delta$ shows a slight decrease after sample containing HA above 7 phr.

Diffusion studies

Effect of filler loading

The transport of solvents through the elastomer materials depends on the nature and loading of filler, interfacial interaction and morphology of the system, temperature, etc. The effect of various loadings of nanohydroxyapatite on the transport properties of polymer composites is characterized by their swelling behavior in industrial solvents such as petrol, kerosene and diesel. The solvent sorption of CI-NB/HA nanocomposites has assessed by calculating their mol percentage uptake (Q_t) using Eq. (1)

$$Q_t = \frac{(M_t/M_s)}{M_p} \times 100 \quad (1)$$

where M_t represents the mass of solvent absorbed at a given time 't,' M_s is the molar mass of the solvent, and M_p is the mass of elastomer matrix. Figure 8 represents the sorption curves (Q_t Vs. \sqrt{t}) of petrol through CI-NBR/HA nanocomposites for varying nanohydroxyapatite contents. It is clearly seen from all the curves that an initial increase in solvent uptake is speedy due to the large concentration gradient of the solvent and the mass of the absorbed solvent levels off near the saturation equilibrium. Also, the percentage of weight gain is much reducing in nanocomposites than that of the chlorinated rubber. The decreased sorption of filled composites can be explained in terms of the homogenous dispersion of nanoparticles in the rubber matrix. The strong polar interaction at the interface along with the C–C covalent bond formed as a result of DCP vulcanization restricts both the local segmental mobility and long-range movements of rubber chain which creates a tortuous path for the transport of the penetrant molecules [34]. Further, it is to be noticed that

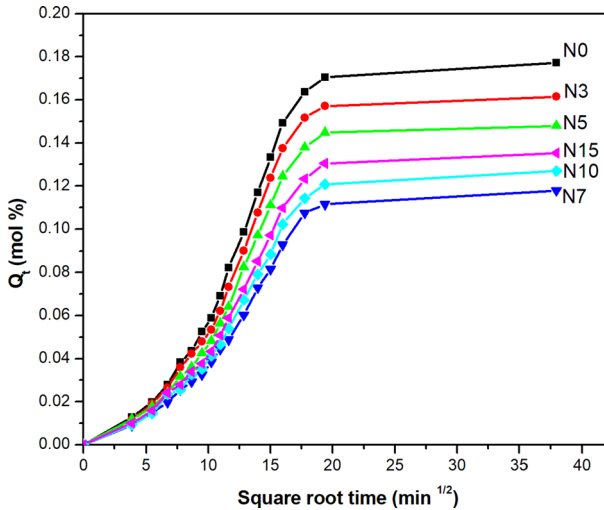


Fig. 8 Solvent uptake of different contents of HA-filled CI-NBR in petrol

beyond 7 phr the solvent uptake increased slightly which indicates the effective reinforcement in the composite occurs up to 7 phr of HA content. The slight increase in sorption beyond 7 phr HA-loaded samples is due to the agglomeration of nanohydroxyapatite which is evident from the SEM micrographs. The diffusion trend is the same for other industrial solvents under this study [35].

Effect of penetrant size

Solvent properties such as structure, molecular weight and polarity seem to exert a considerable effect on sorption phenomena. The percentage uptake of petrol, kerosene and diesel by CI-NBR/7 phr HA is given in Fig. 9. Here, petrol shows higher sorption than that of kerosene and diesel and the equilibrium sorption trend observed in the order petrol > kerosene > diesel. This can be explained on the basis of the size and molecular weight of probe molecules. The molar volume of petroleum fuels taken follows the order of petrol < kerosene < diesel. Based on free volume theory, the penetration of molecules mainly depends on the free volume inside the matrix so that the penetrants can easily exchange the position of polymer chain segments. As the penetrant size increases, the exchange of chain segments becomes difficult and that needs more energy, particularly in the case of nanoparticles-filled rubber compounds [36].

Effect of temperature

The mol percentage uptake of CI-NBR nanocomposite containing 7phr HA is compared at various temperatures by conducting the experiments at 27, 40 and 50°C in petrol. From the figure (Fig. 10), it is obvious that the amount of solvent uptake and thus the diffusion rate increases as the temperature is increased.

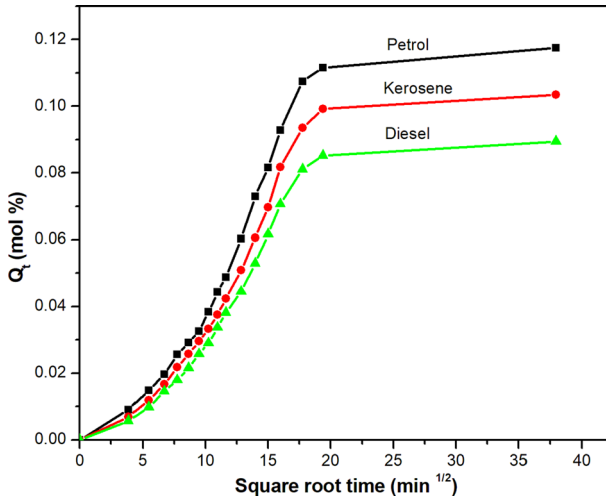


Fig. 9 Solvent uptake of Cl-NBR/7 phr HA in different petroleum fuels

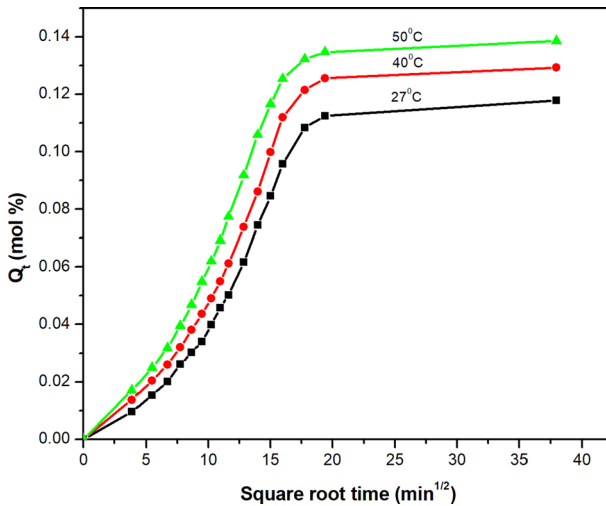


Fig. 10 Solvent uptake of Cl-NBR/7 phr HA in petrol at different temperatures

Similar diffusion behavior is observed with other industrial solvents also. This is due to the combined effect of increased segmental mobility of the elastomer chain and kinetic energy of penetrant molecules. This will lead to the weakening of filler matrix adhesion, and thus, the voids generated will increase the free volume of the system.

Kinetic parameters

The transport properties such as diffusion, sorption and permeation coefficients have been evaluated for the system in order to study the nature of interfacial interaction between CI-NBR and HA.

Diffusion coefficient (D)

The diffusivity D of the rubber nanocomposites is measured using the equation [37]

$$D = \pi \left(\frac{h\theta}{4Q_\infty} \right)^2 \quad (2)$$

where h is the initial sample thickness, θ is the slope of the linear portion of the sorption curve of the plot of % Q_t versus \sqrt{t} , and Q_∞ is the equilibrium absorption. The estimated values of D for the nanocomposites are given in Table 1 for industrial solvents. It is obvious from the table that the diffusion coefficient of nanocomposite greatly reduced as compared to the bare CI-NBR and a systematic decrease is observed up to the nanocomposite with 7 phr HA, after that a slight increase in D value is observed. The solvent diffusion through the nanocomposite materials is a kinetic parameter which depends on the concentration, orientation, size distribution and interaction of filler with the matrix at the interface [38]. The diffusion of probe molecules through a membrane occurs due to random motions of the individual molecules. As the solvent molecule diffuses into the elastomer matrix, the system will expand and weaken the molecular interaction between the chains. However, the nanoparticles-reinforced matrix restricts chain flexibility. The evenly dispersed nanoparticles orient in a regular manner in the macromolecular chain which decreases the free space inside the system [39]. Also, the high aspect ratio of the nanofiller ensures better interfacial adhesion which further reduces the D values for the nanocomposite. The minimum value of the diffusion coefficient for the CI-NBR/7 phr HA is attributed to its maximum reinforcement effect due to optimum crosslink

Table 1 Diffusion, sorption and permeation values of CI-NBR/HA nanocomposites in petroleum fuels

Samples	Diffusion coefficient $D \times 10^5$ (cm ² /s)			Sorption coefficient (S)			Permeation coefficient $P \times 10^5$ (cm ² /s)		
	Petrol	Kerosene	Diesel	Petrol	Kerosene	Diesel	Petrol	Kerosene	Diesel
N0	3.12	3.09	3.06	1.61	1.38	1.04	5.023	4.264	3.182
N3	3.09	3.04	3.01	1.56	1.32	1.01	4.820	4.013	3.040
N5	3.01	2.93	2.89	1.51	1.28	0.99	4.545	3.750	2.861
N7	2.87	2.81	2.76	1.32	1.17	0.86	3.788	3.288	2.374
N10	2.92	2.89	2.85	1.38	1.23	0.96	4.029	3.555	2.736
N15	2.98	2.94	2.91	1.40	1.24	0.98	4.158	3.645	2.852

density. Also, diffusivity decreases when going from petrol to diesel in case of fuels due to the increased molar volume.

Sorption coefficient (S)

The diffusion of industrial solvents such as petrol, diesel and kerosene through Cl-NBR/HA can be explained in terms of sorption coefficient (S), and it can be measured using Eq. (3)

$$S = \frac{W_{\infty}}{W_p} \quad (3)$$

where W_{∞} is the mass of the solvent at equilibrium swelling and W_p is the mass of the polymer sample. The S value obtained for equilibrium swelling data is presented in Table 1. From the table, it can be seen that the sorption coefficient decreased with increase in the filler loading and the lowest value is obtained for nanocomposite containing 7 phr HA. This may be due to the regular orientation of nanoparticles in the polymer matrix which retard the penetration of solvent molecules.

Permeation constant (P)

Since the permeation of the penetrant into an elastomer membrane is a combination of the diffusivity as well as sorptivity, the permeation coefficient (P) has been computed as the product of diffusion and sorption coefficients as

$$P = D \times S \quad (4)$$

The permeation constant values obtained for the Cl-NBR/HA are also given in Table 1. It is followed that P value shows the same trend as that of D and S with respect to filler loading. Sample with filler loading 7 phr shows minimum permeability due to the increased chain packing densities which decreased the free volume available in the matrix to accommodate the penetrant molecules. However, above 7 phr loading of fillers, there is an increase in permeation due to aggregation of nanofiller which decreases the interfacial adhesion.

Arrhenius parameters

From the temperature dependence of D , P and S , the activation energy needed for the process of diffusion, E_D or permeation E_p of the solvent molecules was computed using Arrhenius equation [34]

$$X = X_0 e^{-(E_a/2.303RT)} \quad (5)$$

where X can be D or P and X_0 is D_0 or P_0 , R is the universal gas constant, and T is the temperature.

The estimated E_D and E_p values obtained from the diffusion data are displayed in Table 2. These values are found to be increasing with the loading of nanoparticles

Table 2 E_P (KJ/mol) and E_D (KJ/mol) values of Cl-NBR/HA nanocomposites in petroleum fuels

Samples	Petrol		Kerosene		Diesel	
	E_P	E_D	E_P	E_D	E_P	E_D
N0	5.18	3.92	5.57	4.21	5.72	4.26
N3	5.36	4.06	5.65	4.26	5.78	4.29
N5	5.43	4.09	5.74	4.31	5.87	4.34
N7	5.73	4.18	6.05	4.49	6.1	4.5
N10	5.66	4.16	5.96	4.44	6.05	4.46
N15	5.59	4.15	5.88	4.41	5.96	4.43

and also with the molecular size of the penetrant molecules. Besides the high aspect ratio of nanoparticles, the dipolar attraction between chlorine segment of Cl-NBR and –OH group of HA leads to enhanced matrix–filler interaction resulting in enhanced reinforcement. Cl-NBR/7phr HA has the highest activation energy which can be explained on the basis of maximum reinforcement and greater crosslink density in this sample. As filler content increases above 7 phr, the homogeneity of the distribution of filler decreases which creates voids in the interface and lesser energy may be required for the percolation of solvent molecules.

Thermodynamic parameters

The equilibrium sorption constant K_s has been determined from the amount of liquid sorbed by a given mass of rubber. Mathematically, it is the ratio of number of moles of solvent sorbed at equilibrium to the mass of the polymer sample.

Using the values of K_s , the enthalpy of sorption ΔH_s and entropy ΔS_s can be determined by van Hoff equation

$$\text{Log}K_s = \left(\frac{\Delta S}{2.303R} \right) - \left(\frac{\Delta H_s}{2.303RT} \right) \quad (6)$$

The value of ΔH_s and ΔS_s of sorption for industrial fuels is given in Table 3. The table clearly depicts that all the samples show positive ΔH value in all the solvents.

Table 3 ΔH , ΔS and ΔG values of Cl-NBR/HA nanocomposites in petroleum fuels

Samples	ΔH (KJ/mol)			ΔS (J/mol)			$-\Delta G$ (KJ/mol)		
	Petrol	Kerosene	Diesel	Petrol	Kerosene	Diesel	Petrol	Kerosene	Diesel
N0	1.28	1.38	1.46	28.74	26.45	23.08	7.342	6.555	5.464
N3	1.31	1.39	1.49	24.73	23.28	21.97	6.109	5.594	5.101
N5	1.34	1.44	1.53	22.99	20.88	20.17	5.557	4.824	4.521
N7	1.52	1.56	1.61	19.89	18.31	15.41	4.447	3.933	3.013
N10	1.49	1.53	1.58	20.74	19.68	17.74	4.732	4.374	3.742
N15	1.44	1.47	1.53	21.25	20.02	19.06	4.935	4.536	4.188

That is the sorption follows an endothermic reaction pathway. The positive ΔS values indicate that the penetrant molecules sorbed are retained as liquid structures within the rubber. The feasibility of sorption process has been ascertained by calculating the Gibbs free energy of the process by the equation

$$\Delta G_s = \Delta H_s - T\Delta S \tag{7}$$

The free energy (Table 3) values are influenced by the loading nanoparticles, and the maximum value is obtained for Cl-NBR/7phr HA, indicating a decrease in spontaneity upon filler addition. This may be because the tortuosity of penetrant molecule increases through the highly packed nanohybrid vulcanized samples.

Mechanism of sorption

To investigate the sorption mechanism, the solvent uptake results of the nanocomposites are fitted to the equation

$$\text{Log}\left(\frac{Q_t}{Q_\infty}\right) = \log k + n \log t \tag{8}$$

where Q_t and Q_∞ are the respective mass uptake of solvents at time t and equilibrium, k and n are constants. The k values given in Table 4 (for petroleum fuels) depend on the structural characteristics of the matrix and measures the extent of interaction between the rubber and solvent [40]. On comparing with the unfilled rubber all the filled samples show lower k value, and in the case of composite, this value slightly decreases with increase in nanoparticles up to optimum loading (7 phr) and then a slight increase is obtained, indicating lower rubber-solvent interactions due to the insertion of nano-HA. The values of n propose the mechanism of sorption. The value of n is 0.5 for normal Fickian mode of transport where the rate of chain relaxation is greater compared to the diffusion rate of the solvent. When the chain relaxation becomes slower than the rate of diffusion, then n value reaches unity and the transport approaches non-Fickian behavior. If the value of n is in between 0.5 and 1, the mode of sorption is said to be 0.5 and 1. It is noted that the values of n vary from 0.5 to 1 and clearly point out an anomalous mode of transport. It is well established

Table 4 n and k values of Cl-NBR/HA nanocomposites in petroleum fuels

Samples	Petrol		Kerosene		Diesel	
	n	k (min ⁻¹)	n	k (min ⁻¹)	n	k (min ⁻¹)
N0	0.74	0.17	0.79	0.13	0.78	0.13
N3	0.78	0.14	0.84	0.11	0.82	0.11
N5	0.79	0.14	0.85	0.10	0.84	0.10
N7	0.82	0.12	0.89	0.06	0.87	0.05
N10	0.80	0.15	0.87	0.07	0.86	0.07
N15	0.78	0.16	0.86	0.08	0.85	0.08

that the macromolecular chain relaxation decreases with the degree of reinforcement and becomes comparable with the concurrent penetrant diffusion rate.

Conclusions

Chlorinated NBR/hydroxyapatite nanocomposites were prepared by an open mill mixing technique. The FTIR study confirmed the interaction between rubber and HA nano-filler through the shift in position and presence of HA particles at 567 cm^{-1} . The XRD characterization confirmed the existence of XRD peak of HA in the polymer with a decrease in amorphous domain. The SEM images revealed the insertion of nanoparticles into the macromolecular chain with a uniform dispersion of fillers. The thermal stability of Cl-NBR/HA nanocomposites was significantly larger than that of the virgin polymer due to the reinforcing of nanoparticles into the polymer chains. The results from LOI measurements indicated that the addition of HA to rubber could impart excellent fire resistance which can be suitable for the fabrication flame-retardant materials. The dielectric constant of all the samples decreased with the frequencies and reached a constant value at a higher frequency. The maximum dielectric constant was observed for the sample with 7 phr HA loading. Diffusion, permeation and sorption coefficient of HA-filled rubber decreased as a function of the increase in loading of filler. The activation energy for the diffusion of the penetrant molecule was found to be higher of composites than pristine polymer. The minimum solvent swelling was noted for 7 phr loading of HA particles.

Funding The author (M.T. Ramesan) greatly acknowledge the financial assistance from KSCSTE, Government of Kerala, India (Order No.566/2017/KSCSTE).

Compliance with ethical standards

Conflict of interest The authors of this article have no conflict of interest to declare.

References

1. Khobragade PS, NaikChatterjee JBA (2017) Polystyrene-grafted wollastonite nanofiller for styrene butadiene rubber nanocomposite: rheological, thermal and mechanical studies. *Polym Bull* 74:1915–1934
2. Abbasian M, Seyyedi M, Jaymand M (2020) Modification of thermoplastic polyurethane through the grafting of well-defined polystyrene and preparation of its polymer/clay nanocomposite. *Polym Bull* 77:1107–1120
3. Sadeghalvaad M, Dabiri E, Zahmatkesh S, Afsharimoghadam P (2019) Preparation and properties evaluation of nitrile rubber nanocomposites reinforced with organo-clay, CaCO_3 , and SiO_2 nanofillers. *Polym Bull* 76:3819–3839
4. Suhailath K, Ramesan MT (2019) Investigations on the structural, mechanical, thermal and electrical properties of Ce doped TiO_2 /poly (n-butyl methacrylate) nanocomposites. *J Therm Anal Calorim* 135:2159–2169

5. Vijayan PP, Puglia D, Pioteck J, Kenny JM, Thomas S (2015) Liquid-rubber-modified epoxy/clay nanocomposites: effect of dispersion methods on morphology and ultimate properties. *Polym Bull* 72:1703–1722
6. Zaragoza MV, Yescas AY, Arellano EAJ, Cruz AA, Saguilan AA, Vargas ER, Guzman SS, Valdes SS (2014) Immobilization of TiO₂ nanoparticles on montmorillonite clay and its effect on the morphology of natural rubber nanocomposites. *Polym Bull* 71:1295–1313
7. Zhu S, Guo J, Zhang J (2018) Enhancement of mechanical strength associated with interfacial tension between barium titanate and acrylonitrile–butadiene rubber with different acrylonitrile contents by surface modification. *J Appl Polym Sci* 135:45936–45946
8. Jasna VC, Anilkumar T, Naik AA, Ramesan MT (2018) Chlorinated styrene butadiene rubber/zinc sulfide novel nanocomposites with unique properties- structural, flame retardant, transport and dielectric properties. *J Polym Res* 44(144):1–14
9. Gatos KG, Kocsis JK (2007) Effect of the aspect ratio of silicate platelets on the mechanical and barrier properties of hydrogenated acrylonitrile butadiene rubber (HNBR)/layered silicate nanocomposites. *Eur Polym J* 43:1097–1104
10. Lapa VLC, de Oliveira PD, Visconte LLY (2008) Investigation of NBR-cellulose II nanocomposites by rheometric and equilibrium swelling properties. *Polym Bull* 60:281–290
11. Balachandran M, Bhagawan SS (2017) Mechanical, thermal, and transport properties of nitrile rubber–nanocalcium carbonate composites. *J Appl Polym Sci* 126:1983–1992
12. Yang S, Tian J, Bian X, Wu Y (2020) High performance NBR/fly ash composites prepared by an environment-friendly method. *Compos Sci Technol* 186:107909
13. Kim J, Oh T, Lee D (2003) Preparation and characteristics of nitrile rubber (NBR) nanocomposites based on organophilic layered clay. *Polym Int* 52:1058–1063
14. Jasna VC, Priyanka K, Mathew G, Ramesan MT (2018) Evaluation of spectral, thermal, flame retardant, dielectric, solvent diffusion and transport behavior of novel nanocomposite derived from chlorinated styrene butadiene rubber and manganous tungstate. *Polym Compos* 39(S3):E1880–E1889
15. Armentano I, Dottori M, Fortunati E, Mattioli S, Kenny JM (2010) Biodegradable polymer matrix nanocomposites for tissue engineering: a review. *Polym Degrad Stab* 95:2126–2146
16. Boudemagh D, Venturini P, Fleutot S, Cleymand F (2019) Elaboration of hydroxyapatite nanoparticles and chitosan/hydroxyapatite composites: a present status. *Polym Bull* 76:2621–2653
17. Dong QX, Chen QJ, Yang W, Chen Q, Yang W, Zheng Y, Liu X, Li Y, Yang M (2008) Thermal properties and flame retardancy of polycarbonate/hydroxyapatite nanocomposite. *J Appl Polym Sci* 109:659–663
18. Bhowmik R, Katti KS, Katti DR (2009) Molecular interactions of degradable and non-degradable polymers with hydroxyapatite influence mechanics of polymer-hydroxyapatite nanocomposite biomaterials. *Int J Nanotechnol* 6:511–529
19. Velazco LIC, Nonell JM, Valdes SS, deValle LFR (2009) Morphology and osteogenetic characteristics of polyamide/ nanohydroxyapatite biocomposites. *Polym Bull* 62:99–110
20. Nihmath A, Ramesan MT (2018a) Synthesis, characterization, processability, mechanical properties, flame retardant and oil resistance of chlorinated acrylonitrile butadiene rubber. *Polym Adv Technol* 29:2165–2173
21. Nihmath A, Ramesan MT (2018b) Preparation, characterization, thermal and electrical properties of chlorinated EPDM/hydroxyapatite nanocomposites. *Polym Compos* 39:2093–2100
22. Pang YX, Bao XJ (2003) Influence of temperature, ripening time and calcination on the morphology and crystallinity of hydroxyapatite nanoparticles. *Eur Ceram Soc* 23:1697–1704
23. Nejadi E, Firouzdoz V, Eslaminejad MB, Bagheri F (2009) Needle-like nano hydroxyapatite/poly(L-lactide acid) composite scaffold for bone tissue engineering application. *Mater Sci Eng C* 29:942–949
24. Guozhang WuG, Li B, Song J (2011) Enhancing the electrical and thermal stability of metallic fiber-filled polymer composites by adding tin–lead alloy. *Polym Bull* 67:1105–1110
25. Devi RR, Gogoi K, Konwar BK, Maji TK (2013) Synergistic effect of nanoTiO₂ and nanoclay on mechanical, flame retardancy, UV stability, and antibacterial properties of wood polymer composites. *Polym Bull* 67:1105–1110
26. Suhailath K, Thomas M, Ramesan MT (2020) Effect of temperature on AC conductivity of poly (butyl methacrylate)/cerium dioxide nanocomposites and applicability of different conductivity modeling studies. *Res Chem Intermed* 46:2579–2594

27. Hadi JM, Aziz SB, Mustafa MS, Brza MA, Hamsan MH, Kadir MFZ, Gharee HO, Hussein SA (2020) Electrochemical impedance study of proton conducting polymer electrolytes based on PVC doped with thiocyanate and plasticized with glycerol. *Int J Electrochem Sci* 15:4671–4683
28. Aziz SB, Karim WO, Gharee HO (2020) The deficiency of chitosan: AgNO₃ polymer electrolyte incorporated with titanium dioxide filler for device fabrication and membrane separation technology. *J Mater Res Technol* 9:4692–4705
29. Abdullah OG, Salman YAK, Saleem SA (2016) Electrical conductivity and dielectric characteristics of in situ prepared PVA/HgS nanocomposite films. *J Mater Sci Mater Electron* 27:3591–3598
30. Aziz SB, Al-Zangana S, Brza MA, Saeed SR, Abdulwahid RT, Kadir MFZ (2019) Study of dielectric properties and ion transport parameters in chitosan-barium nitrate based solid polymer electrolytes. *Int J Electrochem Sci* 14:11580–11595
31. Aziz SB, Karim WO, Brza MA, Abdulwahid RT, Saeed SR, Al-Zangana S, Kadir MFZ (2019) Ion transport study in CS: POZ based polymer membrane electrolytes using Trukhan model. *Int J Mol Sci* 20:5625
32. Aziz SB, Marif RB, Brza MA, Hamsan KMFZ (2019) Employing of Trukhan model to estimate ion transport parameters in PVA based solid polymer electrolyte. *Polymers* 11:1694
33. Mousa A, Ishiaku US, Ishak ZAM (2005) Resistance of dynamically vulcanized poly(vinyl chloride)/nitrile butadiene rubber thermoplastic elastomers. *Polym Bull* 53:203–212
34. Sareena C, Sreejith MP, Ramesan MT, Purushothaman E (2015) Transport properties of coconut shell powder (CSP) reinforced natural rubber composites in aromatic solvents. *Polym Bull* 72:1683–1702
35. Padhi S, Achary PGR, Nayak NC (2015) Molecular transport behaviour of organic solvents through halloysite nanotubes filled ethylene–vinyl acetate copolymer. *Bull Mater Sci* 38:925–933
36. Jasna VC, Ramesan MT (2018) Preparation, characterization, dielectric properties and solvent imbibing behavior of styrene butadiene rubber/zinc sulfide nanocomposites. *Int J Plast Technol* 23:217–223
37. Thomas SP, Thomas S, Mathew EJ, Marykutty CV (2014) Transport and electrical properties of natural rubber/nitrile rubber blend composites reinforced with multiwalled carbon nanotube and modified nano zinc oxide. *Polym Compos* 35:956–963
38. Jasna VC, Anilkumar T, Mathew G, Ramesan MT (2018) Novel nanocomposites based on chlorinated styrene butadiene rubber and manganous tungstate: focus on curing, mechanical, electrical and solvent transport properties. *J Mater Sci* 53:9861–9876
39. LakshmiPriya S, Kumar SA, Nandakumar K, Thomas S (2019) Influence of POSS fillers on the transport properties of natural rubber nanocomposites. *Polym Compos* 40:3020–3031
40. Sen SK, Dasgupta B, Banerjee S (2009) Effect of introduction of heterocyclic moieties into polymer backbone on gas transport properties of fluorinated poly(ether imide) membranes. *J Membr Sci* 343:97–103

Publisher's Note Springer Nature remains neutral with regard to jurisdictional claims in published maps and institutional affiliations.

Affiliations

A. Nihmath¹ · M. T. Ramesan¹ 

¹ Department of Chemistry, University of Calicut, Calicut University P.O., Malappuram, Kerala 673635, India